

## ELLIPTICAL PIN FINS AS AN ALTERNATIVE TO CIRCULAR PIN FINS FOR GAS TURBINE BLADE COOLING APPLICATIONS

### Part 2 : Wake Flow Field Measurements and Visualization Using Particle Image Velocimetry

**Oğuz Uzol \* , Cengiz Camci**  
Turbomachinery Heat Transfer Laboratory  
Department of Aerospace Engineering  
Pennsylvania State University  
University Park, PA 16802

#### **ABSTRACT**

Extensive wake flow field measurements and visualizations are conducted using particle image velocimetry (PIV) inside the wakes of the elliptical and circular pin fin arrays in order to better understand the flow physics and the loss mechanisms of these devices. The true-mean velocity field inside the wake two diameters downstream of the pin fin arrays is obtained by collecting and ensemble averaging a large number of PIV samples in the midplane of the test section. Additional experiments are also conducted inside the very near wake of the pin fins in order to visualize instantaneous flow field features. The results of the study reveal that the circular pin fin array creates a large low momentum wake region when compared to the elliptical pin fin arrays. It is observed from the flow visualization inside the wake that this kind of a very large momentum deficit is created due to the early separation of the flow from the circular fins in the second row. In the case of elliptical fins, however, the flow stays attached to the fin surface and the separation occurs very close to the downstream stagnation point on the surface which in turn results in a very small low momentum wake region behind the elliptical pin fin arrays. The mean turbulent kinetic energy levels from the PIV measurements show very high turbulence levels in the wake of the circular fin arrays compared to the elliptical fins. However, the smaller momentum deficit inside the elliptical pin fin wakes results in higher local Reynolds numbers inside the wake when compared to the circular pin fin wakes. This in turn helps to keep the endwall heat transfer enhancement levels close to the circular fin arrays although the turbulence levels are much lower in this region.

#### **NOMENCLATURE**

D	Circular Fin diameter, Elliptical Fin minor axis length
H	Pin fin height
k	Turbulent kinetic energy
N	Total number of samples used in ensemble averaging
$Re_D$	Reynolds number based on D
S	Pin fin array spanwise spacing
SEF	Standard Elliptical Fin
u	Velocity vector component in x-direction
$\bar{u}$	Ensemble averaged value of the velocity vector component in x-direction
$u'$	RMS component of the velocity vector in x-direction
U	Magnitude of the velocity vector
v	Velocity vector component in y-direction
$\bar{v}$	Ensemble averaged value of the velocity vector component in y-direction
$v'$	RMS component of the velocity vector in y-direction
X	Pin fin array streamwise spacing

#### **INTRODUCTION**

Efficient internal cooling of turbine blades can be achieved by enhancing the heat transfer in internal coolant passages of turbine blades. This can be achieved by increasing turbulence levels and unsteadiness of the coolant flow while keeping the pressure losses as low as possible. In order to produce efficiently cooled

---

<sup>1</sup>Currently at the Department of Mechanical Engineering, Johns Hopkins University, Baltimore MD 21218

turbine blades, determination of the local enhancements of heat transfer and pressure losses as a function of the flow parameters, passage and turbulence promoter geometries is essential. Short cylindrical pin fin arrays are one of the most common cooling devices used for internal heat transfer enhancement purposes inside the turbine blade.

Considerable amount of study has been done in pin fin research. The effects of various parameters on heat transfer and pressure losses have been investigated. Brown et al. [1] performed heat transfer and pressure loss measurements for staggered pin fin arrays in converging ducts in order to simulate the cooling configuration inside the trailing edge region of turbine blades. Different stagger arrangements and trailing edge angles are tested. They compared their results to empirical and theoretical results and it is concluded that more measurements are necessary to obtain a closer understanding of that kind of flow inside the trailing edges. Heat transfer coefficients on pin fin and endwall surfaces were measured for different stagger arrangements of short pin fin arrays over a Reynolds number range from 300 to 60000 by VanFossen [2] and the data were compared to the data for longer pins. The results showed that the heat transfer coefficients were significantly higher than those for a plain channel with no pins and the heat transfer for short pin fins was lower than that of longer pin fins. Metzger and Haley [3] investigated the character of streamwise heat transfer development in ducts with uniform staggered arrays of both non-conducting and conducting circular pin fins for Reynolds numbers between 1000 and 100000. Some endwall flow visualization is also conducted in this research. Highly three dimensional flow features are present near the endwall in the vicinity of the cylinders, including a saddle point region, a full cylinder radius upstream from the pin fin leading edge. The effects of array geometry and position in an array on an individual pin fin have been investigated by Simoneau and VanFossen [4]. Endwall heat transfer was not considered in this study. It is found that adding a single row of in-line pin fins upstream of a row containing a heated cylinder resulted in an increased heat transfer on the fin about 50%. However adding up to five more rows did not cause any increase or decrease in the heat transfer. Adding 1 to 5 staggered rows upstream caused an increase in heat transfer levels changing between 21% and 64% where the minimum level of enhancement is for 1 upstream row and the maximum enhancement occurred for 2 upstream rows. The study by Metzger et al. [5] is focused on the row-resolved heat transfer variations for both uniform and non-uniform (abrupt pin fin diameter changes) staggered arrays of pin fins in both constant cross-sectional and converging ducts. Their results showed that the heat transfer levels reach a maximum at the third to fifth row and then gradually decline through the remainder of the array. The turbulent heat transfer and friction characteristics in pin fin channels with trailing edge ejection holes are investigated by Lau et al. [6]. This kind of arrangement is commonly found in modern internally cooled turbine blades.

Chyu et al. [7] investigated the effects of non-axial flow entry on pin fin array heat transfer performance for both in-line and staggered arrangements using an analogous mass transfer technique. Their results show that large variations in heat transfer across the rows are created due to highly non-uniform flow distributions. The differences in heat transfer coefficient between the pin and the endwall in pin fin heat transfer was determined by Al Dabagh and Andrews [8] for a staggered pin fin array and for 3 different H/D ratios. Results show that the wall heat transfer was always greater by 15-35% than the pin for the same velocity and Reynolds number. More recently Hwang and Lui [9] reported their measurements of endwall heat transfer and pressure drop inside a trapezoidal duct with in-line pin fin arrays. A review of heat transfer and pressure loss data for staggered arrays of pin fins in turbine cooling applications is performed by Armstrong and Winstanley [10].

This study is an extension of the endwall heat transfer and total pressure loss measurements for elliptical pin fin arrays performed by Uzol and Camci [11]. The objective of the study is to conduct high resolution flow field measurements and visualizations using particle image velocimetry (PIV) inside the wakes of the elliptical and circular pin fin arrays in order to better understand the flow physics and the loss mechanisms of these devices. The experiments are performed for two different Reynolds numbers, 10000 and 47000, based on the inlet velocity and the fin diameter and at the midplane of the test section. Additional experiments are also conducted inside the very near wake of the bottom fin in the second row in order to visualize instantaneous flow field features. Although the three dimensional effects may be significant for these short ( $H/D=1.5$ ) pin fin configurations, current two dimensional measurements at the midplane of the test section will provide invaluable information about the wake flow physics and flow structures for circular and elliptical pin fin arrays.

## EXPERIMENTAL SETUP AND PROCEDURE

The experiments are conducted at the “Low Speed Heat Transfer Research Facility” of the Turbomachinery Heat Transfer Laboratory at the Pennsylvania State University. Detailed information about the facility is presented in Uzol and Camci [11]. The PIV measurements are performed inside the wakes of the circular, standard elliptical fin (SEF) and N fin (Derived from the NACA four digit symmetrical airfoil series) arrays with  $H/D = 1.5$  which is a typical value for turbine blade cooling applications ( Armstrong and Winstanley [10]). The pin fin arrays are placed inside the test section in a staggered array configuration consisting of 2 rows of fins, with 3 fins in the first row and 2 fins in the second row as illustrated in Figure 1. The transverse and streamwise distance between each fin is taken equal to the diameter of the circular fin such that  $S/D = X/D = 2$ . The flow field is divided into five separate PIV measurement domains in

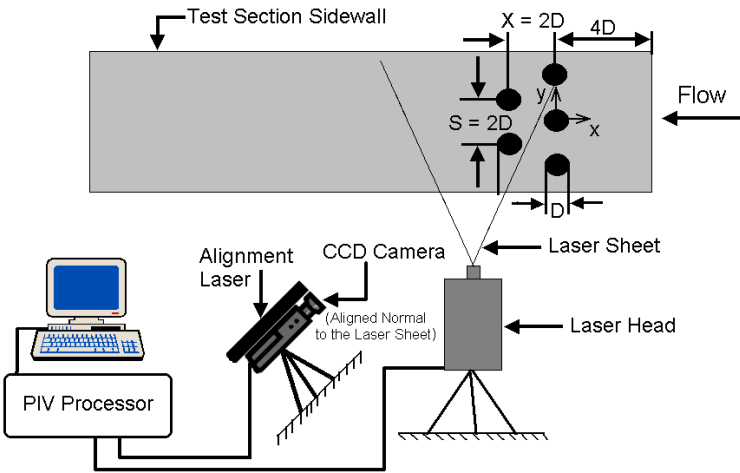


Figure 1. Experimental Setup for PIV Measurements

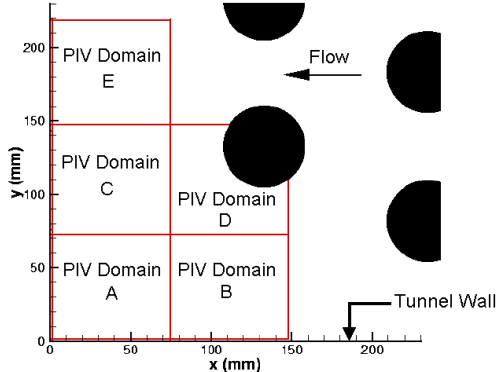


Figure 2. PIV Measurement Domains

the midplane of the test section, covering the half width of the tunnel and up to 2D downstream of the second row in the array. The experimental setup and the PIV measurement domains are illustrated in Figures 1 and 2, respectively. PIV domains A, C and E are used for obtaining the mean flow field 2D downstream, whereas domains B and D are used for visualization of the near wake of the models.

The flow field is seeded with fog particles with particle sizes varying from  $0.25 \mu\text{m}$  to  $60 \mu\text{m}$ . The PIV measurement domains are illuminated from the bottom of the tunnel test section by a double-cavity frequency-doubled pulsating Nd:YAG laser sheet which has an emitted radiation wavelength of 532 nm and 50 mJ per pulse energy level. Pairs of speckle images of the PIV domains are captured using a 1k x 1k pixel Kodak Megaplus ES 1.0 cross-correlation CCD camera which is fully synchronized with the pulsating laser sheets and positioned normal to the laser sheet. In order to make sure the camera is normal to the light sheet, a small 10 mW Helium-Neon laser, with an aperture

attached at the end where laser light is emitted, is placed side by side with the camera. A mirror is placed on the test section sidewall and the reflected laser beam is aligned with the incident beam to make sure that the laser beam (and hence the camera) is at right angles to the sidewall. Since the Nd:YAG laser sheet is positioned such that it is parallel to the tunnel sidewall, this procedure also made sure that the camera is positioned normal to the Nd:YAG laser sheet. The laser sheet pulse separation values are  $25 \mu\text{s}$  and  $15 \mu\text{s}$  for Reynolds numbers 10000 and 47000, respectively. These values are obtained through a systematic method which is explained in detail in Uzol [12].

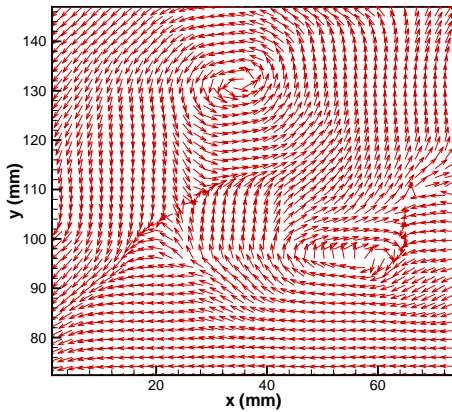
Once the camera and the laser sheet are aligned, the flow field is seeded and the pulse separation is determined, then image pairs of the PIV domains are recorded at 1.25 Hz (max camera frame rate is 15 Hz) to ensure statistically independent sampling and 700 image pairs are collected for PIV domains A, C and E. The number of images collected for each PIV domain is determined through an extensive statistical analysis of the PIV measurements which is explained in detail in Uzol [12]. The uncertainty levels for 700 samples for the mean values of the  $u$  and  $v$  components of the velocity vector are determined to be  $\pm 2.7\%$  and  $\pm 8.2\%$ , respectively. The image maps are then divided into  $32 \times 32$  pixel interrogation areas and 25% overlap is used which generated 1722 vectors in each vector map. All 700 image pairs for the PIV domains A, C and E are cross-correlated, peak-validated, moving averaged/filtered and then ensemble averaged in order to obtain the true-mean flow field inside the wakes of the pin fin arrays. Additionally, 30 image pairs are also collected separately for all PIV domains using the maximum frame rate, 15 Hz, for instantaneous flow field visualization purposes. These image pairs are also cross-correlated, peak-validated, moving averaged/filtered and used as instantaneous flow field data.

## RESULTS AND DISCUSSION

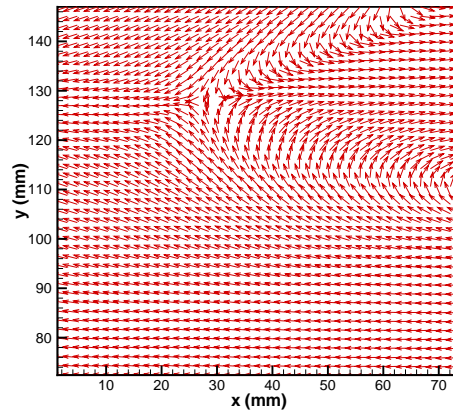
After all 700 images are collected, cross-correlated, moving averaged/filtered, the mean flow field is obtained by ensemble averaging over 700 samples for PIV domains A, C and E. The mean values for the  $x$  and  $y$  components of the velocity vector for each and every interrogation area in the vector map are calculated using

$$\bar{u} = \frac{1}{N} \sum_{i=1}^N u_i \quad (1)$$

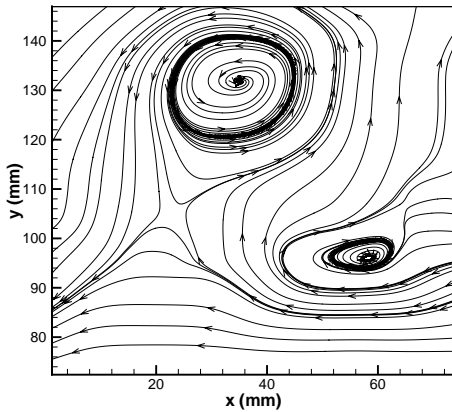
$$\bar{v} = \frac{1}{N} \sum_{i=1}^N v_i \quad (2)$$



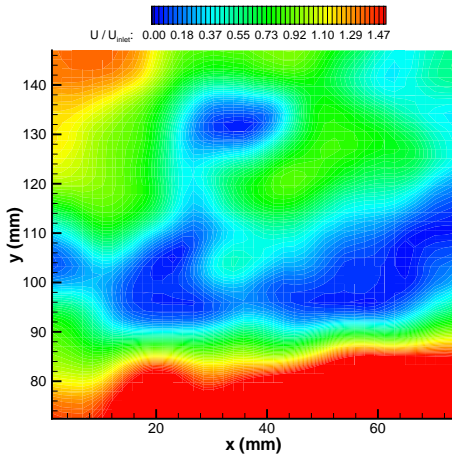
Velocity Vectors



Velocity Vectors

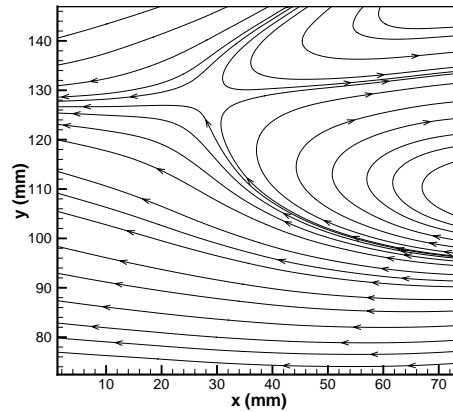


Streamlines

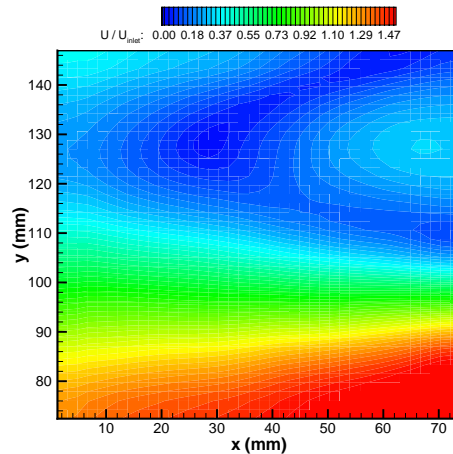


Speed Contours

(a)



Streamlines



Speed Contours

(b)

Figure 3. Measured (a) Instantaneous and (b) Mean Flow Field Inside the Wake of the Circular Fin Array (PIV Domain C)

where N is the total number of samples used in the ensemble averaging process which is 700 for the current experiments. The rms components of the velocity vectors are calculated from

$$u' = \left( \frac{1}{N-1} \sum_{i=1}^N (u_i - \bar{u})^2 \right)^{1/2} \quad (3)$$

$$v' = \left( \frac{1}{N-1} \sum_{i=1}^N (v_i - \bar{v})^2 \right)^{1/2} \quad (4)$$

The meaning of these outputs from the statistical calculations of the PIV vector maps should be considered carefully. The velocity vector map in PIV measurements is an average over the interrogation region. The actual size of the interrogation region used in the current experiments is 2.4 mm corresponding to 32 pixels. This is 4.7% of the diameter of the circular fin. This interrogation area size may be relatively large if the details of the small scale turbulent structures are tried to be measured. However, it is small enough to determine the details of the large scale turbulence present inside the wakes of the pin fin arrays, which is the intended purpose of the current PIV experiments.

The experiments are performed for two different Reynolds numbers, 10000 and 47000. However, the results presented in the figures are the non-dimensionalized results by inlet conditions. Figure 3 shows a comparison of the instantaneous and mean flow fields inside the wake of the circular fin array for PIV domain C. The instantaneous results reveal the details of the vortical structures present inside the wake due to the continuous vortex shedding process from the circular fin array. However the instantaneous details of the flow field disappear when the ensemble averaging is performed. The mean flow fields only show the extent of the low momentum wake region and the steady state shape of the wake. Nevertheless, this kind of mean flow field information is very useful in obtaining and comparing the mean wake characteristics of the circular, SEF and N fin arrays.

Figure 4 shows the measured mean speed contours and streamlines inside the wakes of the circular, SEF and N fin arrays. The difference between the wake characteristics of the pin fin arrays is clearly visible from this figure. It is seen that the circular fin array creates a huge low momentum wake region when compared to the SEF and N fin arrays as illustrated with the blue regions in the speed contour plots. The separation on the circular fins at the second row occurs very early and causes a large low momentum zone inside the wake. The flow acceleration between the two fins in the second row and also between the fins and the bottom wall is much higher for the same inlet conditions in the case of circular fin arrays, creating very high momentum regions

compared to the flow fields for the SEF and N fin arrays, as indicated by the red regions on the speed contour plots in Figure 4. This is mainly due to the blunt geometry of the circular fins which causes a rapid acceleration and deceleration of the flow just above the fin surface because of the sharp drop in the surface pressure. In the case of SEF and N fin arrays the flow acceleration is much lower. The flow separation occurs very close to the trailing edge of the fins creating a very small low momentum wake region. This is the main reason that the SEF and N fin arrays have very low total pressure loss levels compared to the circular fin arrays as discussed in Uzol and Camci [11].

The mean turbulent kinetic energy and vorticity contours are presented in Figure 5. The rms components of the mean velocity vector are used for the calculation of the turbulent kinetic energy, hence

$$k = \frac{1}{2} (u'^2 + v'^2) \quad (5)$$

The turbulent kinetic energy levels inside the wake of the circular fin array is much higher than the levels for the SEF and the N fin arrays. The turbulence generation mainly occurs at the shear layers created due to the acceleration of the flow between the two pins in the second row. This generated turbulence is carried and diffused further downstream resulting in elevated turbulence levels inside the wake over the heater strip where end-wall heat transfer experiments were conducted (Uzol and Camci [11]). The high turbulence levels in this region is the main mechanism of heat transfer enhancement on the wall inside the wake which was measured to be 25% more in average than the levels for the SEF and N fin arrays. Figure 6 shows the mean velocity and the turbulent kinetic energy profiles inside the wakes of the circular, SEF and N fin arrays. These distribution are obtained on the mid section of the PIV domains A, C and E. These results further reveal the differences in the wake characteristics of the pin fin arrays. There exists a big velocity defect region in the wake of the circular fin array. This velocity defect is much smaller for SEFs and even smaller for N fins. The accelerated region between the fins and also between the fins and the wall is also visible for the circular fins.

The instantaneous flow field inside the very near wake of the bottom fin in the second row of the circular, SEF and N fin arrays is illustrated in Figures 7 and 8, showing the results of the measurements for the PIV domain D. The early separation from the circular fin is clearly visible. The velocity vectors around the SEF and the N fin are almost parallel to the surface of the fins following contour of the fin geometry. However for the circular fin the vectors around the fin are directed away from the body because of the large vortical structures embedded inside the wake. This kind of separation characteristics result in a large low momentum wake zone for the circular fin arrays which in turn

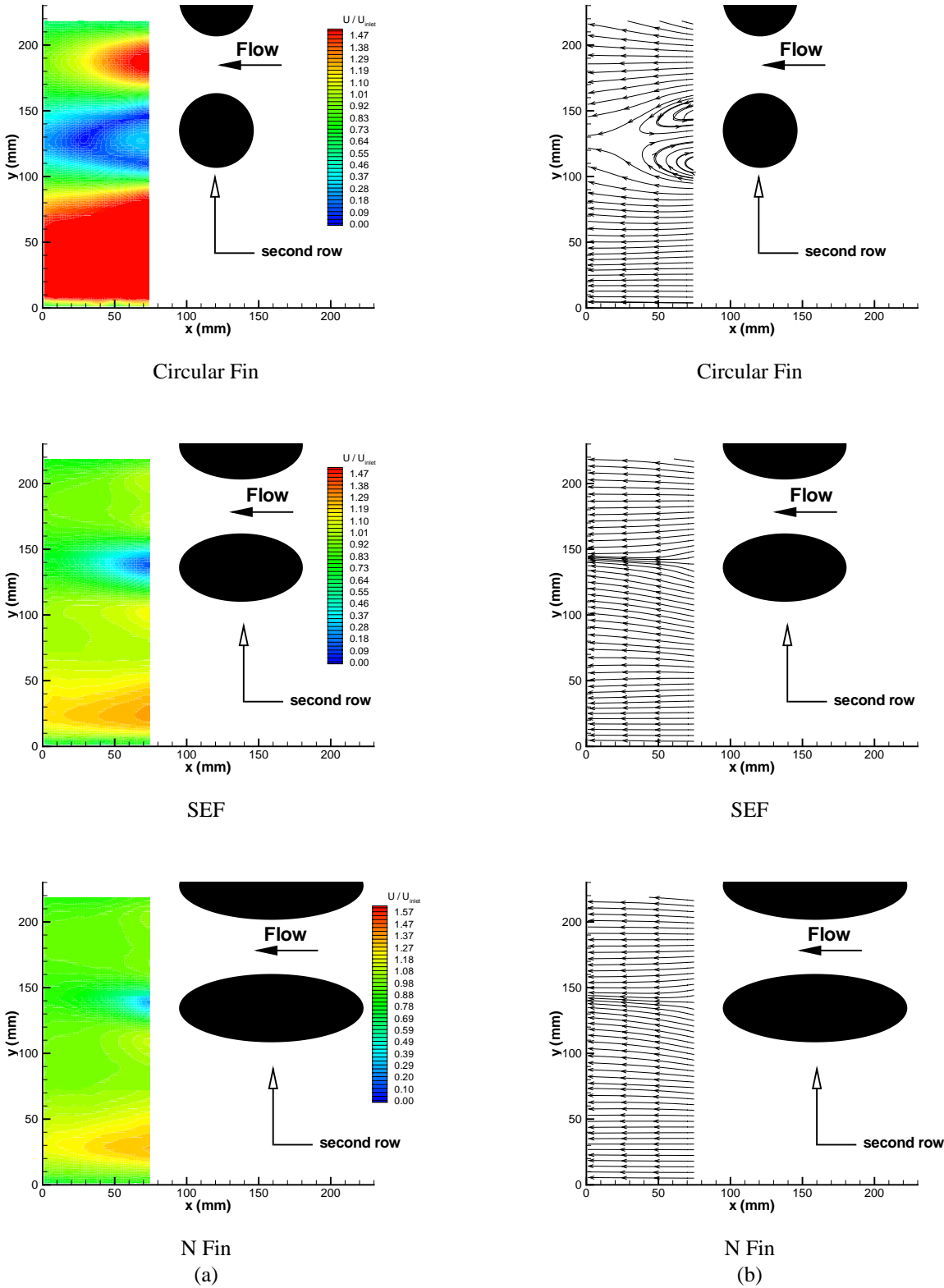


Figure 4. Measured Mean (a) Speed and (b) Streamline Contours for the Circular, SEF and N Fins (PIV Domains A,C and E)

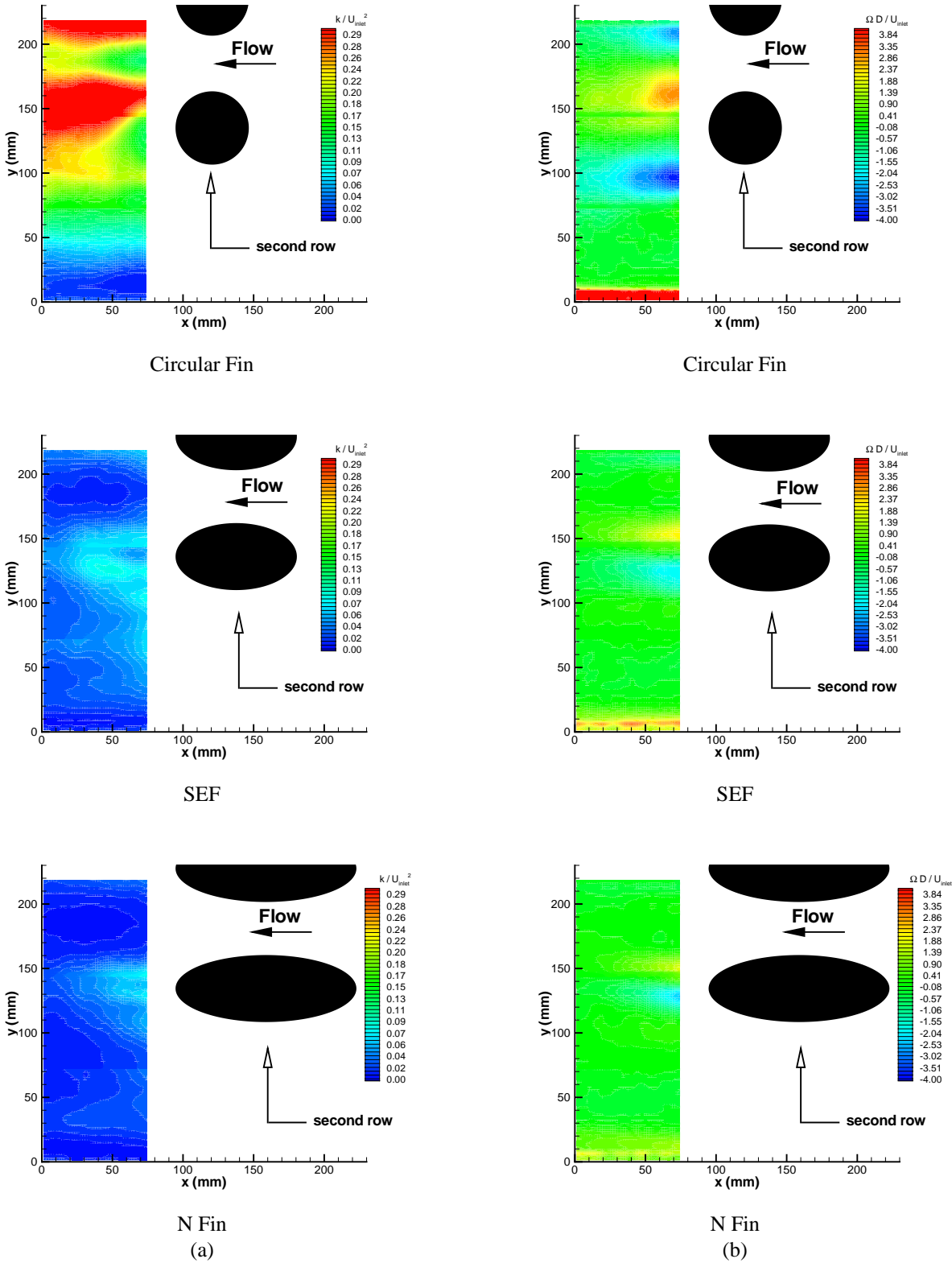


Figure 5. Measured Mean (a)Turbulent Kinetic Energy and (b) Vorticity Contours for the Circular, SEF and N Fins (PIV Domains A,C and E)

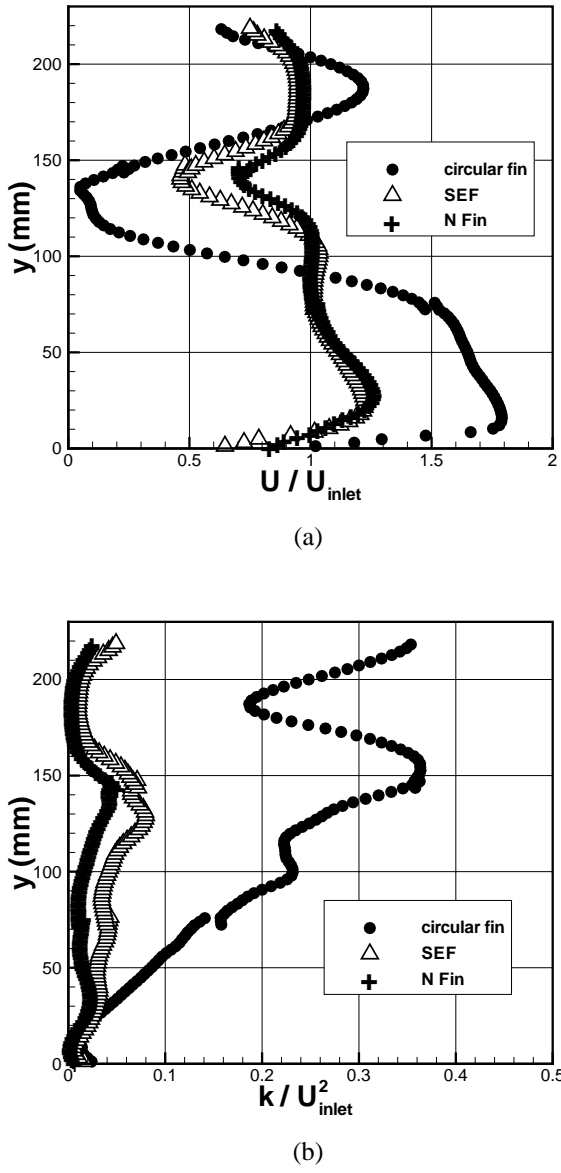


Figure 6. (a) Velocity and (b) Turbulent Kinetic Energy Profiles Inside the Wake for the Mean Flow Field (PIV Domains A, C and E)

results in elevated total pressure loss levels inside the wake. The extend of the low momentum near wake region which is much smaller for the SEF and the N fin arrays is also visualized in these plots. The embedded vortical structures are much smaller and weaker in strength as observed from the vorticity plots in Figure 8. The speed contour plots in Figure 8 reveal that, for the circular fin arrays, the relatively high momentum flow created between the pin fin and the tunnel wall is blocked by the large wake zone and can not get inside this low momentum region.

However in case of elliptical fin arrays, this high momentum flow is able to fill up the wake because of the very small low momentum zone, causing a reduction in the momentum deficit further downstream. This reduction in the momentum deficit results in higher local Reynolds numbers inside the elliptical pin fin wakes compared to the circular pin fin wakes which in turn helps keeping the endwall heat transfer levels of the elliptical pin fin arrays close to the circular pin fin arrays, although the generated turbulence levels are much lower in this region for elliptical pin fin arrays.

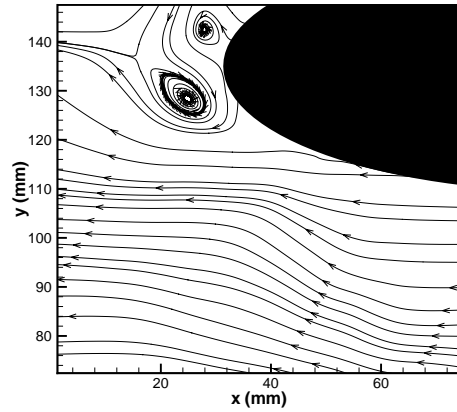
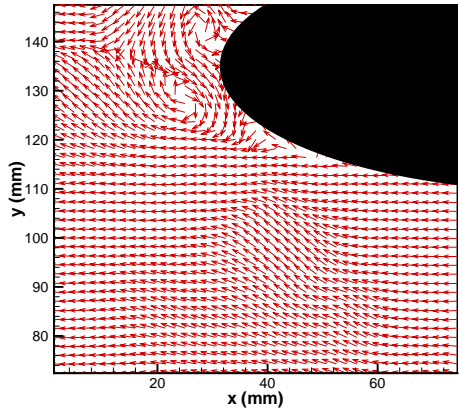
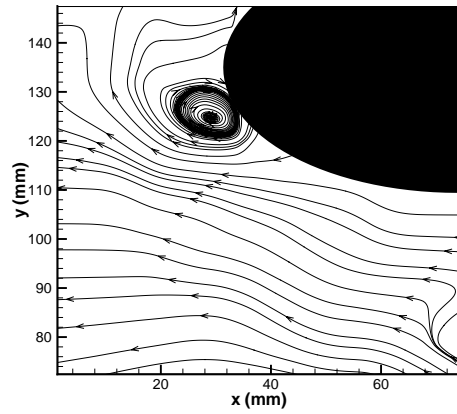
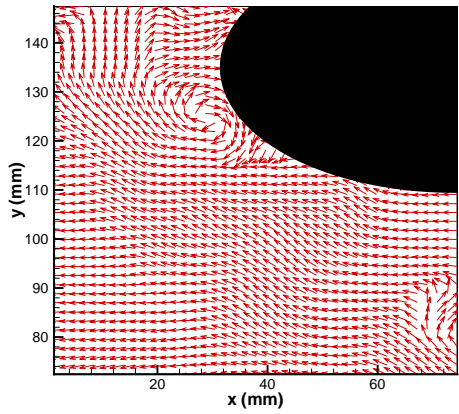
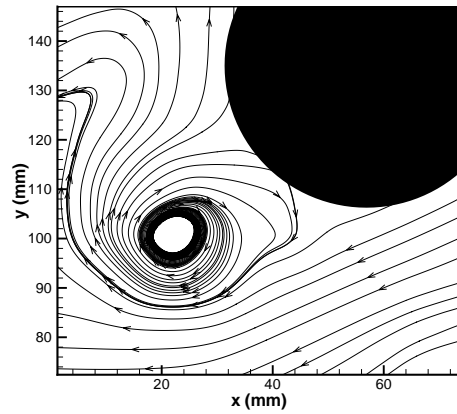
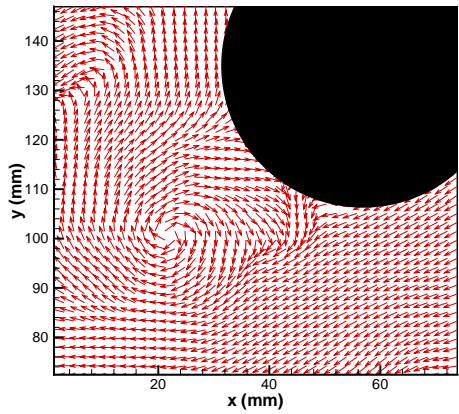
## CONCLUSIONS

Wake flow field measurements and visualizations are conducted using particle image velocimetry (PIV) inside the wakes of the elliptical and circular pin fin arrays discussed in Uzol and Camci [11]. These measurements were extremely useful in understanding the physics behind the pressure loss and heat transfer enhancement mechanisms inside wakes of the elliptical and circular pin fin arrays.

It is observed that the elevated loss levels inside the wake of the circular pin fin array are mainly due to the large low momentum wake region created due to the early separation of the flow from the circular fin surface. However, for the elliptical fin arrays, the flow stays attached to the fin surface and the separation occurs very close to the downstream stagnation point on the surface which in turn results in a very small low momentum wake region behind the elliptical pin fin arrays. This considerable reduction in the size of the wake is the main reason behind the very low total pressure loss character of the elliptical pin fins discussed in Uzol and Camci [11]. The mean turbulent kinetic energy levels from the PIV measurements show very high turbulence levels in the wake of the circular fin arrays compared to the elliptical fins which is essentially the main reason of better endwall heat transfer enhancement characteristics of the circular fin arrays. However, for the elliptical pin fin arrays, the local Reynolds numbers inside the wake are higher than those of the circular fins due to the smaller momentum deficit and this helps keeping the endwall heat transfer enhancement levels close to the circular fins although the turbulence levels are much lower in this region for elliptical pin fins.

## REFERENCES

- [1] Brown, A., Mandjikas, B., Mudyiwa, J. M., 1980, "Blade Trailing Edge Heat Transfer," ASME 80-GT-45.
- [2] VanFossen, G. J., 1982, "Heat Transfer Coefficients for Staggered Arrays of Short Pin Fins," Journal of Engineering for Power, **104**, pp. 268-284.
- [3] Metzger, D. E., Haley, S. W., 1982, "Heat Transfer Experiments and Flow Visualization for Arrays of Short Pin Fins," ASME 82-GT-138.



(a)

(b)

Figure 7. Instantaneous (a) Velocity Vectors and (b) Streamlines Inside the Near Wake of the Circular, SEF and N fins (PIV Domain D)

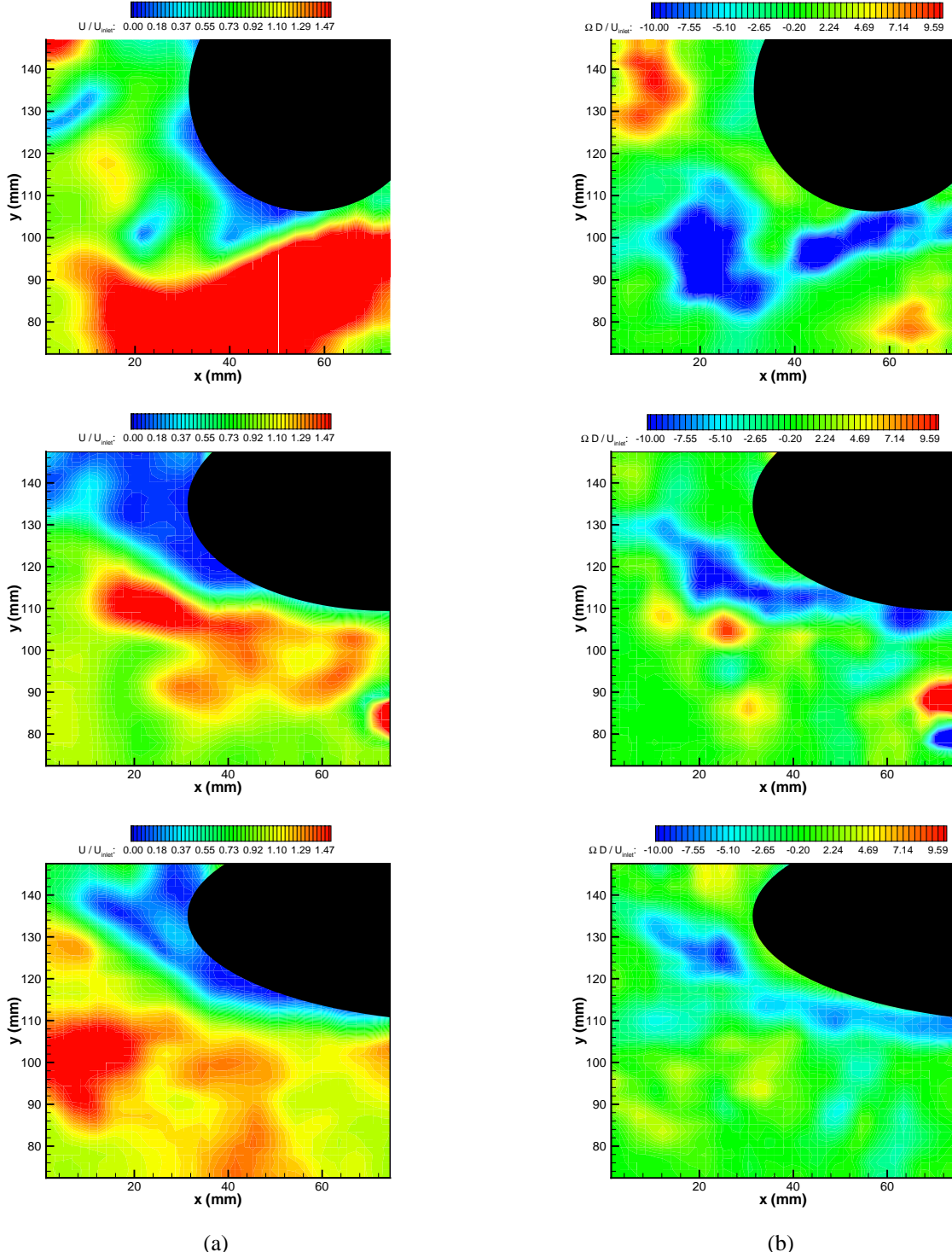


Figure 8. Instantaneous (a) Speed and (b) Vorticity Contours Inside the Near Wake of the Circular, SEF and N fins (PIV Domain D)

- [4] Simoneau, R. J., VanFossen Jr., G. J., 1984, "Effect of Location in an Array on Heat Transfer to a Short Cylinder in Crossflow," *Journal of Heat Transfer*, **106**, pp. 42-48.
- [5] Metzger, D. E., Shepard, W. B., Haley, S. W., 1986, "Row Resolved Heat Transfer Variations in Pin Fin Arrays Including Effects of Non-Uniform Arrays and Flow Convergence," Presented at the International Gas Turbine Conference and Exhibit Dusseldorf, West Germany, 86-GT-132.
- [6] Lau, S. C., Han, J. C., Batten, T., 1989, "Heat Transfer, Pressure Drop and mass Flow Rate in Pin Fin Channels with Long and Short Trailing Edge Ejection Holes," *Journal of Turbomachinery*, **111**, pp. 116-123, 1989
- [7] Chyu, M. K., Natarajan, V., Metzger, D. E., 1992, "Heat/Mass Transfer from Pin Fin Arrays with Perpendicular Flow Entry," *ASME HTD Fundamental and Applied Heat Transfer Research for Gas Turbine Engines*, Vol. 226, pp. 31-39.
- [8] Al Dabagh, A. M., Andrews, G. E., 1992, "Pin Fin Heat Transfer: Contribution of the Wall and the Pin to the Overall Heat Transfer," Presented at the International Gas Turbine and Aero-engine Congress and Exposition Cologne, Germany, 92-GT-242.
- [9] Hwang, J. J., Lui, C. C., 2000, "Detailed Heat Transfer Distribution on the Endwall of a Pin Fin Trapezoidal Duct," *Proceedings of the 8<sup>th</sup> International Symposium on Transport Phenomena and Dynamics of Rotating Machinery, ISROMAC-8*, Vol. 2, pp. 738-745.
- [10] Armstrong, J., Winstanley, D., 1988, "A Review of Staggered Array Pin Fin Heat Transfer for Turbine Cooling Applications," *Journal of Turbomachinery*, **110**, pp. 94-103.
- [11] Uzol, O., Camci, C., 2001, "Elliptical Pin Fins as an Alternative to Circular Pin Fins for Gas Turbine Blade Cooling Applications Part 1: Endwall Heat Transfer and Total Pressure Loss Characteristics," Presented at the 46th ASME International Gas Turbine, Aeroengine Congress and Exposition and Users Symposium, New Orleans, LA.
- [12] Uzol, O., 2000, "Novel Concepts and Geometries As Alternatives to Conventional Circular Pin Fins for Gas Turbine Blade Cooling Applications," Ph.D. Thesis, Pennsylvania State University, University Park, PA.